ACS Infectious Diseases

Featured Article

Cite This: ACS Infect. Dis. 2019, 5, 326−335

pubs.acs.org/journal/aidcbc

Targeting the Bacterial Epitranscriptome for Antibiotic Development: Discovery of Novel tRNA-(N^{1}G37) Methyltransferase (TrmD) Inhibitors

Wenhe Zhong,[†,‡,#] Ann Koay,[§,#] Anna Ngo,[§] Yan Li,[§] Qianhui Nah,[†] Yee Hwa Wong,[‡,∥] Yok Hian Chionh,[†,@] Hui Qi Ng,[§] Xiaoying Koh-Stenta,[§] Anders Poulsen,[§] Klement Foo,[§] Megan McBee,[†] Meng Ling Choong,[§] Abbas El Sahili,[‡,∥] Congbao Kang,[§] Alex Matter,[§] Julien Lescar,[*,†,‡,∥] Jeffrey Hill,[*,§] and Peter Dedon[*,†,⊥]

[†]Antimicrobial Resistance Interdisciplinary Research Group, Singapore-MIT Alliance for Research and Technology, 1 CREATE Way, 138602 Singapore

[‡]NTU Institute of Structural Biology, Nanyang Technological University, 636921 Singapore

[§]Experimental Therapeutics Centre, 31 Biopolis Way, #03-01 Nanos, 138669 Singapore

[∥]School of Biological Sciences, Nanyang Technological University, 60 Nanyang Drive, 637551 Singapore

[⊥]Department of Biological Engineering, Massachusetts Institute of Technology, Cambridge, Massachusetts 02139, United States

Supporting Information

ABSTRACT: Bacterial tRNA modification synthesis pathways are critical to cell survival under stress and thus represent ideal mechanism-based targets for antibiotic development. One such target is the tRNA-(N^{1}G37) methyltransferase (TrmD), which is conserved and essential in many bacterial pathogens. Here we developed and applied a widely applicable, radioactivity-free, bioluminescence-based high-throughput screen (HTS) against 116350 compounds from structurally diverse small-molecule libraries to identify inhibitors of *Pseudomonas aeruginosa* TrmD (*Pa*TrmD). Of 285 compounds passing primary and secondary screens, a total of 61 TrmD inhibitors comprised of more than 12 different chemical scaffolds were identified, all showing submicromolar to low micromolar enzyme inhibitor constants, with binding affinity confirmed by thermal stability and surface plasmon resonance. *S*-Adenosyl-L-methionine (SAM) competition assays suggested that compounds in the pyridine-pyrazole-piperidine scaffold were substrate SAM-competitive inhibitors. This was confirmed in structural studies, with nuclear magnetic resonance analysis and crystal structures of *Pa*TrmD showing pyridine-pyrazole-piperidine compounds bound in the SAM-binding pocket. Five hits showed cellular activities against Gram-positive bacteria, including mycobacteria, while one compound, a SAM-noncompetitive inhibitor, exhibited broad-spectrum antibacterial activity. The results of this HTS expand the repertoire of TrmD-inhibiting molecular scaffolds that show promise for antibiotic development.

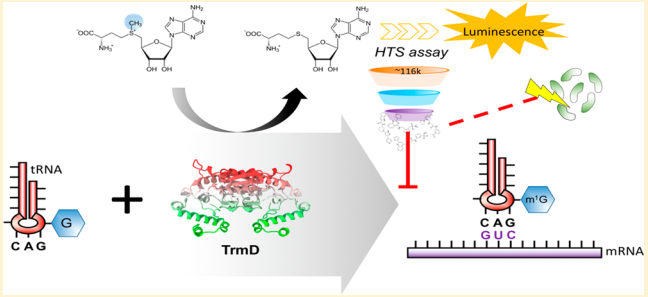

KEYWORDS: *tRNA modification, high-throughput screening, anti-infective development, antibacterial drug screening*

Antimicrobial resistance represents a true crisis with significant societal impact.[1,2] More than 2 million cases of multidrug-resistant (MDR) bacterial infections, including MDR *Pseudomonas aeruginosa*,[3] occur annually and cause ~23000 deaths.[4] Motivated to find new antibiotic chemical scaffolds, we now describe the screening-based discovery of inhibitors of an RNA-modifying enzyme as a target for antibiotic development.

The epitranscriptome consists of 40−50 post-transcriptional modifications of nearly every form of RNA.[5] Transfer RNA (tRNA) modifications play important roles in bacterial pathogenicity,[6,7] with tRNA-modifying enzymes being attractive targets for antibiotic development. For example, the tRNA (guanine 37-N^1)-methyltransferase (TrmD) catalyzes methylation of G37 in tRNA to form m^{1}G37. Essential in most bacteria,[8−11] TrmD differs structurally from its human Trm5 homologue,[12,13] which makes it a prime candidate for an antibiotic target.[12]

Hill et al.[12] discovered and optimized TrmD inhibitors using a fragment screening-based approach targeting the *S*-Adenosyl-L-methionine (SAM)-binding pocket. Though several hits were potent TrmD inhibitors, none showed notable antibacterial activity.[12] Here we developed and applied a bioluminescence-based high-throughput screening (HTS) assay to discover

Received: October 16, 2018
Published: January 25, 2019

DOI: 10.1021/acsinfecdis.8b00275
ACS Infect. Dis. 2019, 5, 326−335

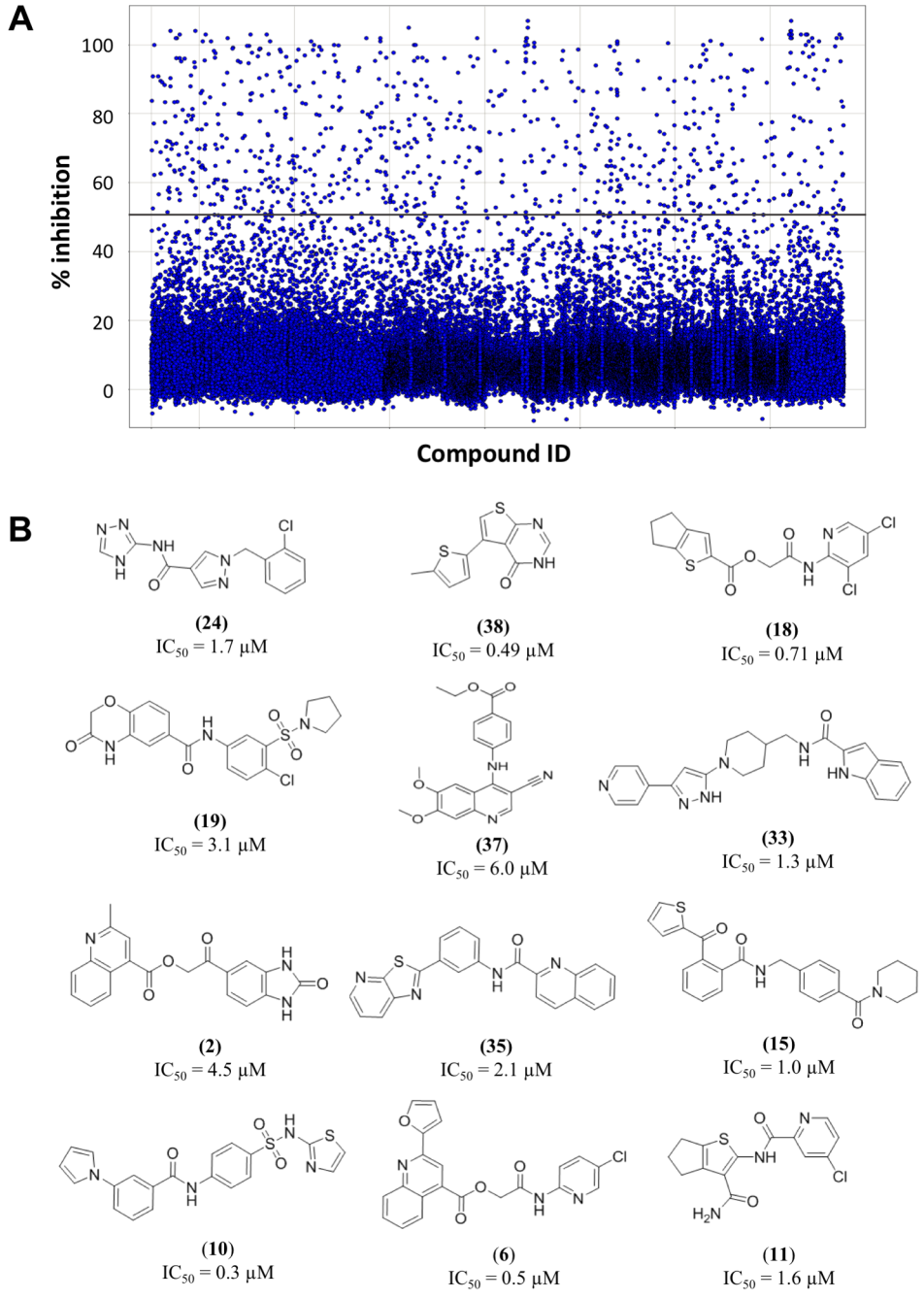

Figure 1. HTS campaign to identify *Pa*TrmD inhibitors. (A) Scatter plot of 116350 compounds screened for TrmD inhibition, expressed as the percent inhibition against the positive control compound Sinefungin. The horizontal line indicates a cutoff applied on TrmD percent inhibition for hit selection. (B) Structures of representative compounds from the different chemical scaffold clusters identified in the HTS campaign. Compound ID numbers in parentheses correspond to ID numbers in Table S3. IC_{50} values represent the activity of the compounds for *Pa*TrmD (see Table S3 for details on other hits in each cluster).

TrmD inhibitors in a 116350-compound library, with several hits showing antibiotic activity.

RESULTS AND DISCUSSION

Development and Application of a HTS Method for Identifying TrmD Inhibitors. On the basis of the workflow in Figure S1, we developed a robust, nonradioactive assay for TrmD activity involving 384-well plates and the Promega MTase Glo system that uses SAH derived from SAM-mediated methylation to drive a coupled bioluminescence reaction. The assay was adapted to a low-volume, HTS format (Table S1) and validated with known methyltransferase inhibitors Sinefungin and Suramin (Figure S2). Their respective half-maximal inhibitory concentrations (IC_{50}) were 8.3 ± 1.1 and 9.1 ± 1.1 μM, respectively, against *Pa*TrmD (Figure S2B), which are comparable to values for other methyltransferases.[12,14] The validated assay was used to screen a 116350-compound library for *Pa*TrmD inhibitory activity at a compound concentration of 12.5 μM (Figure 1A; screening statistics in Table S2). Primary hits (883) were retested, and a counter screen lacking TrmD reduced this set to 285. After the removal of hits previously identified to be frequent hitters in

DOI: 10.1021/acsinfecdis.8b00275
ACS Infect. Dis. 2019, 5, 326−335

Table 1. Enzyme Inhibitory Activities and Binding Properties of Selected Pyridine-Pyrazole-Piperidine Class Inhibitors of *Pa*TrmD

Compound ID	Structure	IC_{50} (μM)	K_i (μM)	K_D (nM)	k_{on} ($M^{-1}s^{-1}$)	k_{off} (s^{-1})
30	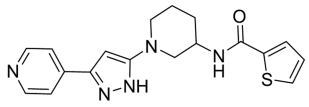	12 ± 3	5.7± 1.4	603	95850 ± 3200	0.0578 ± 0.0009
32	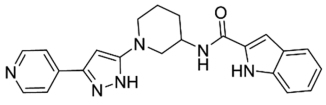	2.9 ± 0.9	1.4± 0.4	999	211200 ± 7700	0.211 ± 0.004
33	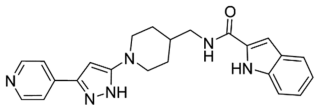	1.3 ± 0.3	0.6± 0.1	837	238000 ± 6300	0.199 ± 0.002

other in-house run HTS campaigns (such as metal chelators, catechol amino acids, and pyrrol-pyrazoles), the 61 remaining hits were structurally clustered by linear hashed fingerprint calculations followed by leader−follower clustering using Canvas.[15,16] Their IC_{50} values were found to range between 0.1 and 14 μM (Figure 1B and Table S3). As shown in Table S3, the 61 hits were comprised of 15 chemical scaffolds shared by at least two compounds and 21 individual structures.

Pyridine-Pyrazole-Piperidine Compounds Bind to TrmD and Increase Thermal Stability. Binding of the 61 hits to *Pa*TrmD was quantified by surface plasmon resonance (SPR) and a thermal stability assay. Most hits did not alter the *Pa*TrmD melting point (T_m) (Table S3). Strikingly, all compounds in the pyridine-pyrazole-piperidine cluster caused significant positive T_m shifts (ΔT_m = 3−7 °C) at compound concentrations from 12.5 to 50 μM (Figure S3), which is consistent with *Pa*TrmD stabilization. SPR analysis of *Pa*TrmD binding by the pyridine-pyrazole-piperidine hits showed nanomolar binding affinities characterized by fast binding kinetics (Table 1 and Figure S4). In addition, the Hill slope values of dose−response inhibitions by pyridine-pyrazole-piperidine compounds are 1.0−1.5 (Table S3), suggesting the binding is reversible. It is noteworthy that the inhibitory constant for compound 30 is much larger than its K_D, where other pyridine-pyrazole-piperidine compounds have similar values for these two parameters, suggesting this compound may have a mechanism different from that of compounds **32** and **33**. These results point to relatively potent *in vitro* inhibition of *Pa*TrmD by diverse scaffolds that cause variable disruption of protein structure, which raises the question of how the hits bind to *Pa*TrmD.

Pyridine-Pyrazole-Piperidine Compounds Compete with SAM. We next sought to determine if compounds **30**, **32**, and **33** competed with the binding of SAM to *Pa*TrmD. IC_{50} values for these compounds were derived at SAM concentrations representing 1, 3, and 9 times the *Pa*TrmD K_m, respectively (2, 6, and 18 μM, respectively; TrmD kinetics in Table S4). At saturating SAM concentrations, IC_{50}'s for **30**, **32**, and **33** increased by ≤10-fold, which suggests competition with SAM (Figure 2A−C and Table S3). These results raised questions about the location of the binding sites for these hits in *Pa*TrmD.

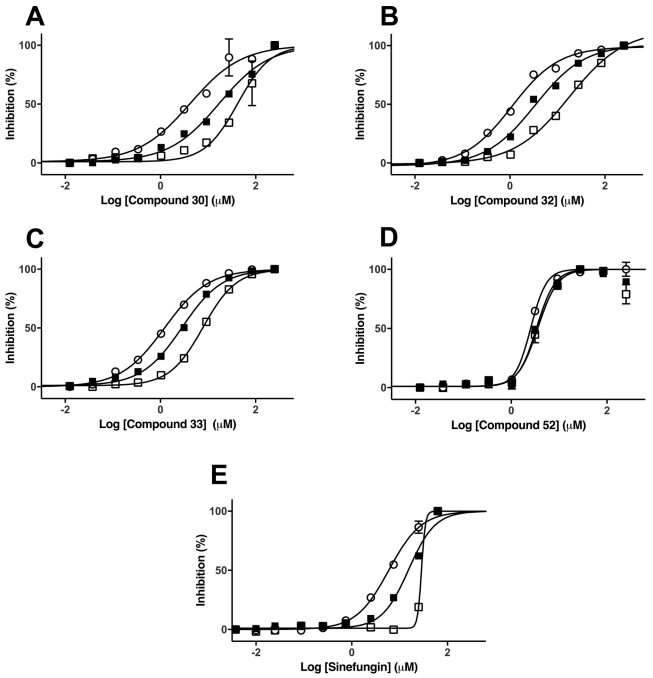

Figure 2. Dose-dependent inhibition of TrmD by HTS hits and Sinefungin at varying SAM concentrations. The IC_{50} values determined for each compound at SAM concentrations of 2 μM (○), 6 μM (■), and 18 μM (□) are (A) 4.2, 17, and 42 μM for compound **30**; (B) 1.1, 3.4, and 17 μM for compound **32**; (C) 1.2, 2.9, and 7.9 μM for compound **33**; (D) 2.6, 3.4, and 3.6 μM for compound **52**; and (E) 5.9, 15, and 29 μM for Sinefungin, respectively. Each data point represents the mean ± the deviation about the mean for N = 2.

Pyridine-Pyrazole-Piperidine Compounds Bind to the SAM Pocket of TrmD. Given evidence of SAM competition, we used nuclear magnetic resonance (NMR) spectroscopy to probe interactions of TrmD with **30**, **32**, and **33**. Here we used the N-terminal domain (NTD) fragment of *Pa*TrmD, which harbors the active site and SAM-binding pocket, binds SAM with high affinity, and generates well-dispersed cross peaks in $^1H-^{15}N$ HSQC spectra.[17] The first task was to delineate the SAM-binding site in NTD. Comparing $^1H-^{15}N$ HSQC spectra

DOI: 10.1021/acsinfecdis.8b00275
ACS Infect. Dis. 2019, 5, 326−335

of NTD with and without SAM (Figure 3A), we found SAM interaction was indicated by chemical shift changes for residues

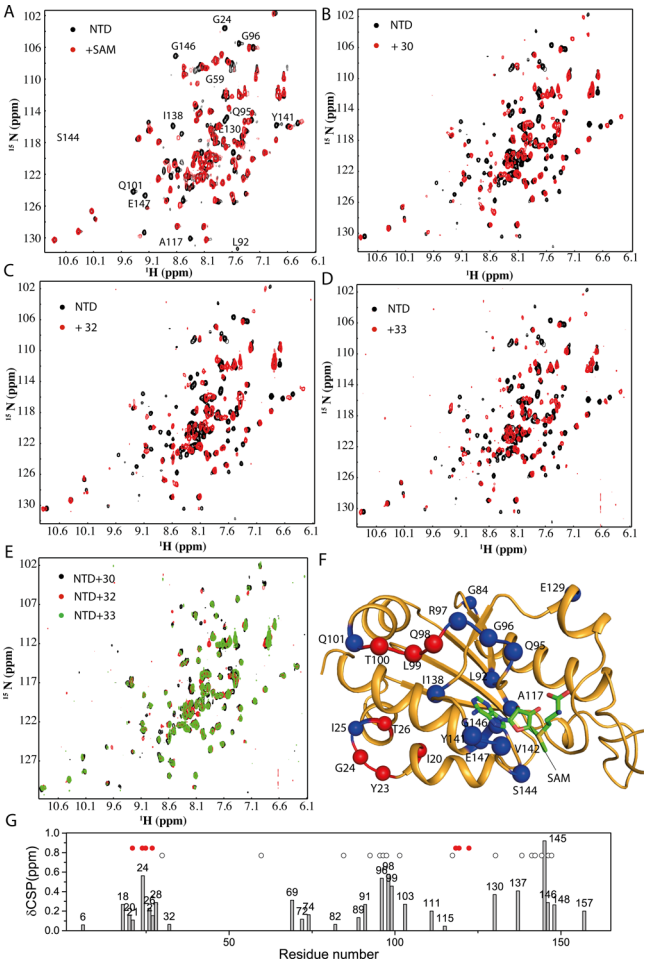

Figure 3. NMR analysis of interactions between NTD and SAM-binding-site compounds. $^{1}H-^{15}N$ HSQC spectra of the *Pa*TrmD NTD in the absence (black) and presence (red) of (A) SAM, (B) compound **30**, (C) compound **32**, and (D) compound **33**. Amino acids affected by SAM binding are labeled. (E) Overlay of the $^{1}H-^{15}N$ HSQC spectra of the NTD in complexes with compounds **30**, **32**, and **33**. (F) Amino acids affected by SAM binding. The structure of NTD was modeled using the *Pa*TrmD−SAM complex (PDB entry 5WYQ)[18] as a template. SAM is shown as sticks. Residues exhibiting line broadening and chemical shift perturbations are shown as blue and red spheres, respectively. (G) Residues affected by compound **30** binding. The averaged chemical shift changes (δCSP) are plotted against the amino acid sequence. Only residues that could be unambiguously assigned are shown. Amino acids exhibiting line broadening and chemical shift changes upon SAM binding are shown as empty and red circles, respectively.

near the SAM-binding pocket (Figure 3F). In the crystal structures discussed below, three active-site loops were conserved and essential for SAM binding in TrmD: the cover, bottom, and wall loops (Figures S5 and S6). The NMR data indicate that several amino acids projecting from these loops are affected by SAM binding: L92, Q95, and G96 in the cover loop, I138, Y141, V142, S144, G146, and E147 in the bottom loop, and A117 in the wall loop (Figure 3F). This confirms that the NTD can be used to localize the binding of hits. Additionally, SAM−NTD interactions underwent intermediate exchange on the NMR time scale, as indicated by line broadening of affected residues (Figure 3G). This suggests micromolar to millimolar binding affinity. In addition to residues near the SAM-binding pocket, other residues such as Q95−T100 also exhibited chemical shift perturbations or line broadening upon SAM binding (Figure 3F), indicating their interactions were undergoing fast or intermediate exchange. In the absence of SAM, size-exclusion chromatography data show that the NTD is a dimer in solution (Figure S7). Our NMR relaxation experiment also showed that this region formed dimers in solution.[17] Interestingly, of the perturbed residues, most not belonging to the SAM-binding site are involved in interactions at the dimer interface in full-length *Pa*TrmD,[18] suggesting that SAM binding could alter the dimer interface to influence the chemical environments of residues from the C-terminal region. Altogether, these results indicate that, in solution, SAM is mainly stabilized by three active-site loops and binding causes global conformational changes that stabilize the NTD dimer, which also agrees with thermal stability results (Figure S8).

Having established binding of SAM to the NTD, we next assessed chemical shift changes caused by binding of **30**, **32**, and **33**. As shown in Figure 3B−D, binding of the pyridine-pyrazole-piperidines produced chemical shift changes similar to those of SAM in $^{1}H-^{15}N$ HSQC spectra of the NTD, indicating that these inhibitors interact in the SAM pocket. Unlike SAM binding, chemical shifts of amino acids perturbed by binding of pyridine-pyrazole-piperidines underwent slow exchange on the NMR time scale, consistent with nanomolar binding by SPR (Table 1 and Figure S4). Overlaying $^{1}H-^{15}N$ HSQC spectra of NTD complexes with the three compounds revealed that they exhibit similar binding modes (Figure 3E), which is not surprising given their common scaffold structures. The partial overlap of affected residues upon SAM and compound binding suggested that the compound-binding site on NTD partially overlapped with SAM. The relationship of the *Pa*TrmD crystal structure to amino acids affected by SAM binding is shown in Figure 3F. Using compound **30** as a reference, the averaged chemical shift perturbations caused by NTD binding were plotted against residue numbers (Figure 3G). This sensitive NMR assay thus identifies the sites of binding of TrmD inhibitors to the NTD.

Structure of the Complex of *Pa*TrmD with 32. X-ray crystallography [2.75 Å (Table 2)] provided a detailed view of the *Pa*TrmD−**32** complex. Compound **32** is clearly resolved at the catalytic site, with the pyridine-pyrazole-piperidine rings deeply buried within the SAM pocket and forming the bulk of protein interactions, while the indole ring points toward the solvent and appears to be more mobile as seen from its higher temperature factors (Figure 4A). Similar to SAM binding in *Pa*TrmD, **32** is mainly stabilized by the three active-site loops (cover, bottom, and wall) (Figure 4A,B): the pyridine-pyrazole rings are tightly bound at the site occupied by the adenine of SAM, making H-bonds with Ile138 and Leu143 (bottom loop); pyridine-pyrazole-piperidine rings further form stacking interactions with Pro94 (cover loop) and Gly145 (bottom loop). The amine next to the pyrazole ring is stabilized by H-bonding with Tyr20 (wall loop). Because the *Pa*TrmD amino acids interacting with **32** are highly conserved among pathogens (Figure S5), the pyridine-pyrazole-piperidine compounds are likely to be broad-spectrum inhibitors of TrmD.

Unlike the "L"-shaped conformation adopted by SAM, with its methyl group projecting toward the tRNA-binding site

DOI: 10.1021/acsinfecdis.8b00275
ACS Infect. Dis. 2019, 5, 326−335

Table 2. Data Collection and Refinement Statistics for the *Pa*TrmD−Compound 32 Complex

PDB entry	6AFK
Data Collection[a]	
space group	$P3_221$
cell dimensions	
a, *b*, *c* (Å)	86.02, 86.02, 149.19
α, *β*, *γ* (deg)	90.00, 90.00, 120.00
solvent content (%)	53
resolution (Å)	74.50−2.75
no. of reflections	185505 (24835)
no. of unique reflections	17233 (2255)
Wilson *B* factor (Å^2)	43.1
R_{merge} (%)	14.3 (120.2)
$I/\sigma I$	14.0 (2.1)
completeness (%)	100.0 (100.0)
multiplicity	10.8 (11.0)
Refinement	
no. of monomers in the asymmetric unit	2
no. of reflections	16300
R_{work}/R_{free}	0.1801/0.2488
no. of non-hydrogen atoms	
protein	3839
water	186
ligands	56
average *B* factor (Å^2)	
protein	62.6
water	56.7
ligands	75.4
root-mean-square deviation	
bond lengths (Å)	0.0083
bond angles (deg)	1.0467
Ramachandran plot	
favored (%)	98.1
allowed (%)	100
no. of outliers	0

[a]Values in parentheses are for the highest-resolution shell.

(Figure S6), **32** adopts a more relaxed conformation, with its indole ring facing the tRNA-binding site (Figure 4C). To investigate the potential interference of **32** in tRNA binding, we modeled the tRNA substrate in the *Pa*TrmD−**32** structure by superimposing the structure of the *Hi*TrmD−tRNA complex (PDB entry 4YVI) (Figure 5A). This produced a model of the ternary complex with a 1.2 Å root-mean-square deviation with the experimental structure for all *α*-carbon atoms. Interestingly, the solvent-exposed indole ring of **32** overlaps with G37 of tRNA, suggesting that **32** not only competes with SAM but also hinders tRNA binding (Figure 5B). In particular, the indole ring forms close contacts with the flexible interdomain linker, which tethers the N- and C-terminal domains, and covers the catalytic site as a structural element that correctly positions and stabilizes tRNA[19] (Figure 5C). In addition, the enzyme inhibitory activity of compound **32** decreased when we increased the tRNA concentration (Figure S9). These observations indicate that **32** competes with both SAM and tRNA and prevents formation of the ternary complex. This dual mode of action may explain its potent inhibition of *Pa*TrmD. Further structural optimization could improve the potency of inhibitors that compete with both SAM and tRNA binding and also target bacterial TrmD with high specificity.

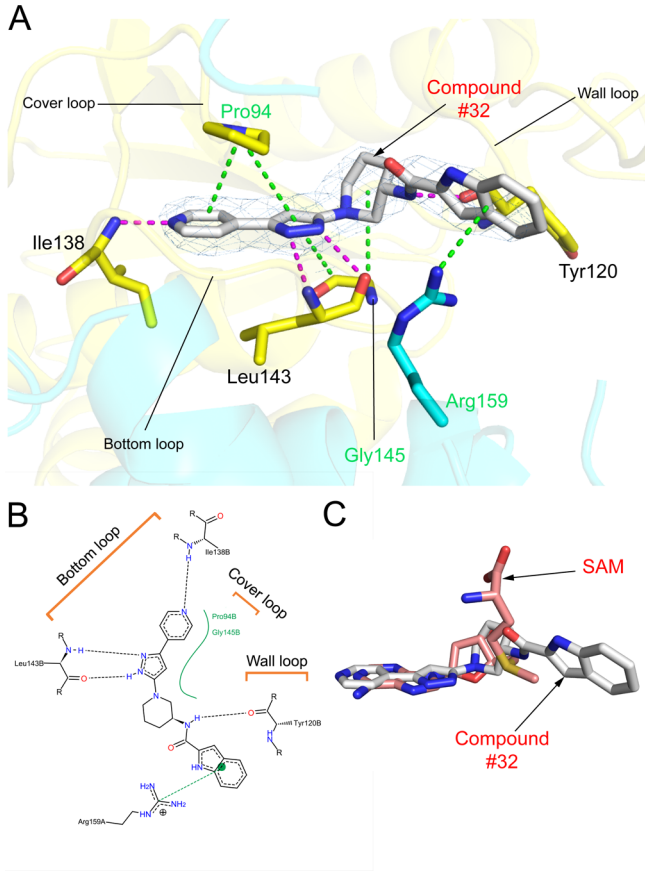

Figure 4. Pyridine-pyrazole-piperidine inhibitor **32** binds in the SAM pocket. (A) Close-up of the catalytic site of *Pa*TrmD showing the binding mode of compound **32**. Polypeptide chains are shown as cartoons (monomer A in cyan and monomer B in yellow), and key interacting residues are shown as sticks. Compound **32** is shown as white sticks with an electron density map (light blue) with Fourier coefficients $2F_o - F_c$, contoured at 1.0σ. Interactions involved in inhibitor binding are indicated by dashed lines (pink, hydrogen bonds; green, hydrophobic contact or π−cation interaction). (B) Schematic drawing showing the inhibitor interactions at the catalytic site. The locations of residues with respect to the three loops that shape the active site are also indicated. (C) Superposition of the present *Pa*TrmD−compound **32** structure with the *Pa*TrmD−SAM complex (PDB entry 5WYQ) in the active site, showing the overlapping binding modes of SAM (salmon) and compound **32** (white). Polypeptide chains have been omitted for the sake of clarity.

Because compound **32** represents a new scaffold for TrmD inhibition, we compared its binding mode with that of the scaffold developed by Hill et al. using a fragment-based approach.[12] We superposed the structure of the complex of *Pa*TrmD with **32** and the structure obtained by Hill et al. of *Hi*TrmD in complex with the TrmD inhibitor AZ38 (Figure S10). Clearly, the pyridine-pyrazole ring of compound **32** overlays well with the thienopyrimidinone ring of AZ38. Both ring groups stay tightly in the adenine pocket between two active-site loops (cover loop and bottom loop). Interestingly, the divergence in ligand binding pose occurs outside the adenine pocket. In *Pa*TrmD, the indole ring of compound **32** is locked in place by π−cation interaction with residue Arg159. In contrast, the imidazole ring of AZ38 is driven away toward the C-terminal domain by interacting with interdomain linker residues Asp169 and Asp177. Without any ligand binding, the interdomain linker is missing due to its high flexibility in the

DOI: 10.1021/acsinfecdis.8b00275
ACS Infect. Dis. 2019, 5, 326−335

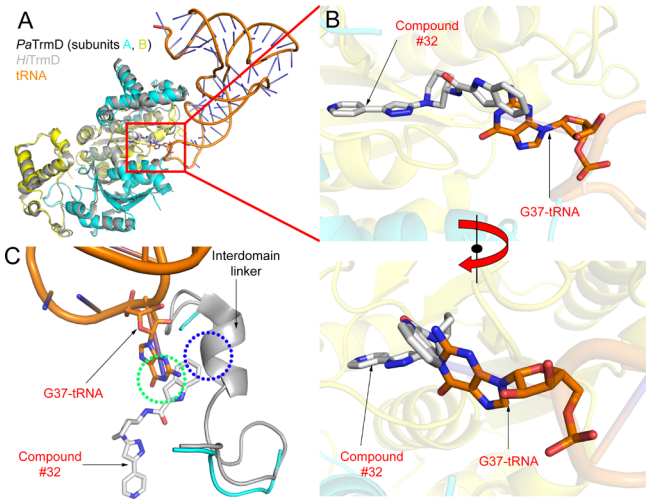

Figure 5. Compound **32** is predicted to hinder the binding of tRNA. tRNA-bound *Haemophilus influenzae* TrmD (PDB entry 4YVI) was superimposed onto the compound **32**-bound *Pa*TrmD structure, based on the Cα atoms. Polypeptide chains of both structures are shown as cartoons (monomer A in cyan and B in yellow for *Pa*TrmD; *Hi*TrmD in gray). The G37 base of the tRNA substrate in the *Hi*TrmD−tRNA structure is shown as orange sticks. (A) Overview of the *Pa*TrmD and *Hi*TrmD superposed structures. (B) Magnified views of the close contact between compound **32** (shown as gray sticks) and G37-tRNA. (C) Summary of the two close contacts between compound **32** and tRNA (circled in green) and between compound **32** and interdomain linker residues 160−169 (circled in blue).

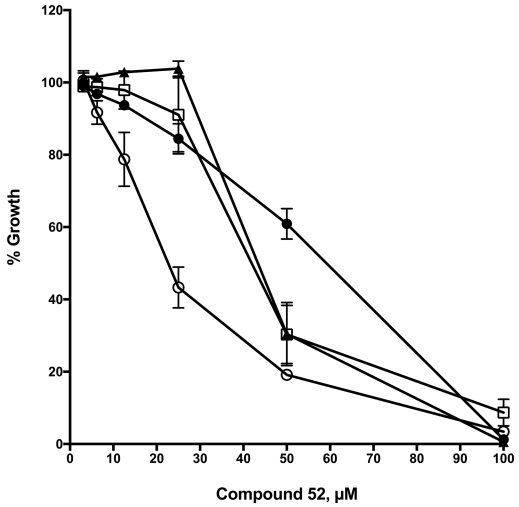

Figure 6. Growth inhibition of *M. bovis* BCG, *M. smegmatis*, *S. aureus*, and *Streptococcus pneumoniae* by compound **52**. The MIC_{50} values for *M. bovis* BCG (○), *M. smegmatis* (●), *S. aureus* (▲), and *St. pneumoniae* (□) are calculated to be 23, 60, 44, and 42 μM, respectively. All data are means ± the standard error of the mean for $N = 3$.

*Pa*TrmD structure. The linker between the pyridine-pyrazole ring and piperidine-indole ring in compound **32** is one carbon shorter than the linker between the thienopyrimidinone ring and phenyl-imidazole ring in AZ38, suggesting the phenyl-imidazole ring in AZ38 is less rigid to be able to interact with the interdomain linker. In the stage of "hit to lead", the chemical linker between ring groups will be a crucial factor for hit optimization. Additionally, the ligand-interacting residues of *Pa*TrmD and *Hi*TrmD are highly conserved, further indicating there is an opportunity to develop universal TrmD inhibitors based on these two scaffolds.

Hits from TrmD Inhibition Screening Show Antibacterial Activity. Given their *Pa*TrmD inhibition potency, the hits from the enzyme inhibition studies were tested for antibacterial activity against a variety of Gram-positive and -negative bacteria, including mycobacteria. As shown in Figure 6 and Table S5, only **7**, **32**, **38**, **51**, and **52** showed growth inhibition. All compounds showed activity against *Staphylococcus aureus*, with **7** and **38** showing additional weak activity against *Mycobacterium bovis* BCG and *Mycobacterium smegmatis*. Notably, **51** and **52** showed greater potency against the mycobacteria, with **52** showing activity against all tested strains (Figure 6 and Table S5). To begin the process of assessing their *in vivo* targets, we tested these compounds against human red blood cells to assess their hemolytic potential as an index of membrane-disrupting potential. None of the compounds showed hemolytic activity at 100 μM (Table S5).

Interestingly, compound **52** {*N*-(3-acetylphenyl)-N^2-[5-chloro-2-(1-pyrrolidinyl)phenyl]glycinamide}, which is not in the pyridine-pyrazole-piperidine scaffold, was identified as a non-SAM-competitive inhibitor (Figure 2D) that did not alter the *Pa*TrmD T_m (Table S3). The fact that compound **52** does not bind in the SAM pocket is supported by that fact that it did not perturb the NMR chemical shifts of the NTD (Figure S10). Efforts to identify the binding site of **52** using X-ray crystallography (crystal soaking) were unsuccessful possibly due to the poor compound solubility [LogP = 3.03, which is higher than the values of pyridine-pyrazole-piperidine compounds (Table S3)]. At this stage, we cannot exclude the possibility that compound **52** could be a nonspecific inhibitor as it has a steep Hill slope (Hill slope of 2.92) (Table S3 and Figure 2D) and shows no effect on the NMR chemical shifts. Further efforts are required to validate this compound, including resynthesis, as a potential new scaffold for TrmD inhibitor development.

■ CONCLUSION

A HTS of 116350 compounds revealed five *Pa*TrmD inhibitors that also showed antibacterial activity against Gram-positive bacteria and mycobacteria. One of these active compounds (**38**) and another biologically inactive hit (**39**) shared the thienopyrimidone scaffold that arose in the fragment-based screen performed by Hill et al.[12] Three other hits showing antibacterial activity (quinolone **7**, pyridinylquinazoline **51**, and pyridine-pyrazole-piperidine **32**) interfered with binding of SAM to *Pa*TrmD, while diarylglycinamide **52** inhibited *Pa*TrmD by another mechanism yet showed activity against Gram-positive pathogens and mycobacteria. Efforts to validate the *in vivo* mechanism of action of these TrmD inhibitors before their further development as antibiotics and to structurally modify them to broaden their activity to Gram-negative pathogens are underway.[20]

■ METHODS

Protein Production. A truncated *Pa*TrmD gene (Leu5−Asp250) was expressed from a pNIC28-Bsa4 construct in *Escherichia coli* BL21 (DE3) Rosetta T1R grown in LB medium (37 °C) and induced with 0.5 mM isopropyl β-D-1-thiogalactopyranoside (16 °C for 24 h). Cell pellets were lysed

DOI: 10.1021/acsinfecdis.8b00275
ACS Infect. Dis. 2019, 5, 326−335

in ice-cold lysis buffer [20 mM Na-HEPES (pH 7.5), 0.3 M NaCl, 10% glycerol, and 0.5 mM TCEP] by sonication. The soluble fraction was obtained by centrifugation, and the supernatant was filtered through a 0.22 μm syringe filter. *Pa*TrmD was purified at 6 °C by IMAC chromatography (HisTrap HP IMAC, GE Healthcare) and by size-exclusion chromatography (SEC, HiLoad Superdex 200 16/60, GE Healthcare) on an ÄKTA system (GE Healthcare). Protein was stored in 20 mM Na HEPES (pH 7.5), 300 mM NaCl, 10% (v/v) glycerol, and 0.5 mM TCEP at −20 °C.

For NMR studies, the N-terminus of *Pa*TrmD (residues 1−167) with a C-terminal His_6 tag (NTD) was expressed from pET29b in *E. coli* grown in M9 medium with 1 g/L $^{15}NH_4Cl$ and 2 g/L [^{13}C]glucose. At an OD_{600} of ∼0.6−0.8, protein expression was induced (0.5 mM IPTG, 18 °C, 12 h). Cells were harvested and suspended in 20 mM phosphate (pH 7.8), 0.5 M NaCl, and 2 mM β-mercaptoethanol, followed by sonication lysis at 0 °C. The lysate was cleared by centrifugation (40000*g*, 20 min, 4 °C), and the supernatant loaded on a Ni^{2+}-NTA column, washed with 20 mM phosphate (pH 7.2), 1.0 M NaCl, 20 mM imidazole, and 2 mM β-mercaptoethanol, and eluted using 500 mM imidazole and 2 mM β-mercaptoethanol. The NTD was purified on a HiPrep 16/60 sephacryl S-200 HR column using 20 mM sodium phosphate (pH 6.5), 150 mM NaCl, and 1 mM DTT. The eluted protein was concentrated to 0.5−0.8 mM (Amicon Centrifugal Filter, 3 kDa molecular weight cutoff).

tRNA Synthesis. $tRNA^{Leu(CAG)}$ was synthesized by *in vitro* transcription (MEGAshortscript T7 Transcription Kit, Thermo Scientific); the DNA template and primers are noted in Table S6 (Integrated DNA Technologies, Inc.). Transcribed tRNA was desalted and purified on an Agilent 1200 HPLC instrument using an Agilent BioSEC-3 column (300 Å pore, 3 μm particle, 7.8 mm inside diameter) at 60 °C with 100 mM ammonium acetate. The purity was determined using an Agilent 2100 bioanalyzer (small RNA chip) and quantified using a Nanodrop spectrophotometer. The final product was desalted in RNase-free water, concentrated to 10−20 mg/mL, and stored at −20 °C.

HTS TrmD Assay. This TrmD assay is based on bioluminescent detection of *S*-adenosyl-L-homocysteine (SAH) production. All assay components were prepared in 50 mM Tris (pH 8), 20 mM NaCl, 2 mM $MgCl_2$, 0.01% (v/v) Triton X-100, and 0.05 mM DTT. The assay began with the addition of 2 μL of 16.5 nM TrmD to predispensed library compounds in 384-well plates (784075-25 Greiner Bio-one) and preincubation at ambient temperature for 30 min. A 2 μL aliquot of a solution containing SAM (4 μM) and $tRNA^{Leu(CAG)}$ (0.8 μM) was then added, and the mixture incubated for 60 min at ambient temperature. TrmD activity was quantified as SAH production using the Methyltransferase-Glo assay kit (Promega). MTase-Glo reagent (diluted 10-fold, 2 μL) was added to the 4 μL reaction mixture for single-concentration screens or to a 4 μL reaction mixture for dose−response studies and incubated for 30 min at ambient temperature. MTase detection reagent (6 μL, diluted 3-fold) was added with incubation for 30 min at ambient temperature before luminescence was read (Tecan M1000 plate reader).

HTS and Dose−Response Studies. For HTS, 384-well small-volume white polystyrene plates were prepared with test compounds dispensed from a stock library by an Echo acoustic dispenser (Labcyte, Sunnyvale, CA). Columns 1 and 2 and columns 23 and 24 were reserved for DMSO and 300 μM Sinefungin, respectively, serving as minimum and maximum inhibition controls, respectively. The primary screen of 116350 compounds was performed at 12.5 μM. For dose−response studies, a 3-fold serial dilution was performed (Bravo liquid handler, Agilent) from stock solutions in 384-well plates (Labcyte). Each dilution series (25 nL) was transferred to the plate in duplicate for the TrmD assay (MultiDrop Combi). The final concentrations of test compounds examined ranged from 0.013 to 250 μM. Plates were centrifuged after each liquid addition step at 300*g* for 3 min to ensure reagent mixing. For hits arising in primary screens, a counter screen assay was performed with 4 μL of 0.2 μM SAH with buffer replacing the TrmD reaction mixture.

Data Management. Screening data were analyzed as the percent inhibition within ActivityBase (IDBS) andf then visualized with SpotFire (TIBCO) to identify hits. TrmD activity was measured as a percentage against the maximum and minimum inhibition controls using eq 1:

$$100\% - \frac{\text{RLU sample} - B}{A - B} \times 100\% \quad (1)$$

where A is the averaged relative luminescence units (RLU) in DMSO control wells (columns 1 and 2) and B is the averaged RLU in Sinefungin control wells (columns 23 and 24). A calculated Z' value[21] of >0.5 for each assay plate was the criterion for quality control. Hits were defined as compounds inhibiting TrmD activity by >50% and were selected from compound stocks for retesting in duplicate alongside a MTase-Glo counter-screen to eliminate false positives based on criteria outlined in Figure S1. Confirmed hits were further validated with reordered compounds from commercially available sources in a 10-point concentration series performed in duplicate. The IC_{50} value, minimum signal, and maximum signal for each compound from the dose−response curve was obtained using a four-parameter logistic fit in the XE module of ActivityBase. K_i values were calculated using the IC_{50}-to-K_i server.[22] The results provided are for competitive inhibition with SAM using the following parameters: [*Pa*TrmD] = 0.008 μM, [SAM] = 2 μM, and apparent K_m(SAM) = 1.8 μM.

Thermal Stability Assay. An inhibitor (12.5−50 μM) and TrmD (7.5 μM) were incubated in 20 mM Tris and 150 mM NaCl (pH 8.0); final DMSO concentrations were ≤2%. Following incubation at ambient temperature for 30 min, SYPRO Orange (Sigma) was added to a 20-fold dilution and duplicates of each reaction mixture were aliquoted into a 384-well LightCycler clear multiwell plate. The plate was sealed and placed in a thermocycler (LightCycler 480 II, Roche) with a thermal ramp rate of 1.8 °C/min applied between 30 and 95 °C and simultaneous measurement of the fluorescence intensity at 465 nm excitation and 580 nm emission. The change in TrmD melting point when the compound was added (ΔT_m) was calculated (LightCycler 480 Software 1.5.0 SP4).

Surface Plasmon Resonance (SPR). SPR studies were performed using a Biacore T200 biosensor (GE Healthsciences). TrmD (∼4000 resonance units) was immobilized by amine coupling to the carboxymethylated dextran matrix of a Series S CM5 chip (GE Healthsciences). Single-cycle kinetic analysis was performed at 25 °C during five injections of the compound at 190 nM and 15 μM. The association time and flow rate were set at 60 s and 30 μL/min, respectively, with 50 mM Na HEPES (pH 7.5), 150 mM NaCl, 0.1% P20, and 3% DMSO as running buffer. K_D was calculated using Biacore T200 Evaluation software (version 2.0, GE Healthsciences).

DOI: 10.1021/acsinfecdis.8b00275
ACS Infect. Dis. 2019, 5, 326−335

NMR. NTD backbone resonance assignments were obtained as described elsewhere.[17] Protein−ligand interactions were analyzed by $^{1}H-^{15}N$ HSQC of 0.4 mM NTD in the absence and presence of 0.8 mM ligands (SAM, inhibitors in water, or DMSO). The averaged chemical shift changes (δCSP) were calculated as described previously.[23]

Crystallization and Data Collection. Crystal screening and optimization for *Pa*TrmD have been described elsewhere.[18] Crystals were soaked with 0.1 mM inhibitor in the precipitating solution supplemented with 20% (v/v) glycerol at 20 °C for 8 h and rapidly frozen in liquid nitrogen. X-ray diffraction data were collected using the MX1 beamline at the Australian Synchrotron. The data set was from a single crystal flash-cooled in liquid nitrogen at 100 K. Diffraction intensities were integrated with MOSFLM[24] and scaled with AIMLESS.[25,26] The data collection and processing statistics are summarized in Table 2.

Structure Determination. The *Pa*TrmD structure was determined by molecular replacement using Phaser.[27] The initial search probe (*Pa*TrmD dimer) for the molecular replacement experiment was obtained from the *Pa*TrmD−SAM structure (PDB entry 5WYQ). The structure was manually refined using Coot[28] followed by several cycles of refinement in REFMAC.[29] Where appropriate, water molecules and ligands were added and TLS refinement was applied at a later stage. Geometrical parameters for ligands were generated using PRODRG.[30] The quality of the structure was assessed using the MOLPROBITY server,[31] and figures were generated using PyMOL.[32] Two-dimensional schematic diagrams of ligand−protein interactions were generated with PoseView.[33,34] Data processing and refinement statistics are summarized in Table 2. Structure factors and coordinates for the *Pa*TrmD−compound **32** complex were deposited in the RCSB Protein Data Bank (www.rcsb.org) as PDB entry 6AFK.

Antibacterial Assay. TrmD inhibitors were first screened at 100 μM against a series of bacteria by monitoring growth in a 96-well plate. *P. aeruginosa* PA1, *Acinetobacter baumannii* clinical isolate, *Klebsiella pneumoniae* ATCC 13883, *Salmonella enteritidis* ATCC 13076, *E. coli* BW25113, and *S. aureus* ATCC 43300 (methicillin-resistant) were tested in cation-adjusted Mueller-Hinton (MH) broth at 37 °C, while *Enterococcus faecalis* ATCC 51299 was tested in brain heart infusion (BHI) broth, and *St. pneumoniae* ATCC 49619 in MH medium supplemented with 3% defibrinated sheep blood (37 °C, 5% CO_2). *M. smegmatis* $mc^{2}155$ was cultured in 7H9 medium.[6] Single colonies were picked from freshly streaked plates, grown overnight (37 °C), subcultured in fresh medium, and further grown (37 °C) to log phase. The cell concentration was adjusted to 10^{5} cells/mL (the inoculum) in each well in the presence or absence of 100 μM test compound (total volume of 100 μL). Ampicillin and kanamycin were used as positive controls. DMSO and blank controls were applied. Cultures were incubated for 22 h before the cell density was read (OD_{600}). For *St. pneumoniae*, cells were pelleted and the supernatant was measured at OD_{450}. The percent survival was calculated from the OD_{600} or OD_{450} value of the test well relative to control wells.

Minimum inhibitory concentrations (MICs) were determined by serial broth microdilution where cell suspensions were incubated with 2-fold serial dilutions of the test compound. The media and inoculum preparations are the same as described above for the screening method. Fresh solutions prepared from powder forms of representative hits **7**, **32**, **38**, **51**, and **52** were used to minimize the risk of degradation. The MIC assay for *M. bovis* bacille Calmette Guérin (BCG) Pasteur strain 1172P2 was performed in flasks at 37 °C with 160 rpm agitation. *M. bovis* BCG was cultured in 7H9 medium. The bacterial inoculum (5×10^{6} colony-forming units/mL) was prepared from glycerol stocks of log-phase bacteria and treated with 2-fold serial dilutions of the test compound. Compound-treated *M. bovis* BCG was cultured for a further 6 days. Measurements were performed on at least two independent experiments in duplicate. The MIC value is determined as the lowest concentration of test compound that prevents bacterial growth. MIC_{50} and MIC_{90} represent hit concentrations inhibiting growth by 50 and 90% as compared to the untreated control, respectively. Both values are determined from the bacterial growth inhibition curve.

Hemolysis Assay. Fresh human red blood cells (RBCs) were washed with PBS until the supernatant was clear. The pellet was resuspended in PBS to an OD_{600} of 24, and 100 μL was added to each well of a 96-well U-bottom plate. Hits were serially diluted in PBS and added (100 μL) to the wells. Triton X-100 was used as a positive control. After incubation for 1 h at 37 °C without being shaken, cells were centrifuged (1000*g*, 15 min). The supernatant was diluted, and OD_{450} measured. Experiments were performed twice.

■ ASSOCIATED CONTENT

Supporting Information

The Supporting Information is available free of charge on the ACS Publications website at DOI: 10.1021/acsinfecdis.8b00275.

Workflow for HTS (Figure S1), positive controls in the TrmD inhibition assay (Figure S2), thermostabilization of TrmD by pyridine-pyrazole-piperidine compounds (Figure S3), binding kinetics of pyridine-pyrazole-piperidine compounds (Figure S4), bacterial TrmD sequence alignment (Figure S5), substrate SAM binding mode in the *Pa*TrmD structure (Figure S6), TrmD protein size estimation in size-exclusion chromatography (Figure S7), thermostabilization of the TrmD NTD by substrate SAM (Figure S8), tRNA competition assay for compound **32** (Figure S9), differences in binding mode between compound **32** and AZ38 determined by Hill et al.[12] (Figure S10), comparison of NMR spectra of the TrmD NTD with and without compound **52** (Figure S11), primary HTS workflow (Table S1), statistics of HTS results (Table S2), list of hits from HTS (Table S3), *Pa*TrmD enzyme kinetics (Table S4), bacterial growth inhibition by selected HTS hits (Table S5), and materials for synthesizing tRNA (Table S6) (PDF)

Accession Codes

Coordinates and structure factors for the *Pa*TrmD−compound **32** complex have been deposited in the Protein Data Bank as entry 6AFK. Compound **32** has been assigned ID number 9WO. The authors will release the atomic coordinates and experimental data upon publication.

■ AUTHOR INFORMATION

Corresponding Authors

*Telephone: +65-690-822-08. E-mail: julien@ntu.edu.sg.
*Telephone: +65-640-703-35. E-mail: jhill@etc.a-star.edu.sg.
*Telephone: +1-617-253-8017. Fax: +1-617-324-5280. E-mail: pcdedon@mit.edu.

DOI: 10.1021/acsinfecdis.8b00275
ACS Infect. Dis. 2019, 5, 326−335

ORCID
Wenhe Zhong: 0000-0002-7617-8345
Anders Poulsen: 0000-0002-2790-9340
Congbao Kang: 0000-0002-9886-9374

Present Address
[@]Y.H.C.: Tychan Pte. Ltd., 80 Robinson Rd., #17-02, Singapore 068898.

Author Contributions
[#]W.Z. and A.K. contributed equally to this work.

Author Contributions
W.Z., A.K., Y.H.C., M.M., and C.K. supervised and performed laboratory work, participated in the design of the studies, and participated in writing the manuscript. W.Z. and Q.N. performed the antibacterial activity and hemolysis assays. W.Z., Q.N., and Y.H.W. purified and crystallized TrmD protein. Y.H.W. and A.E.S. collected the crystal diffraction data. W.Z. and J.L. analyzed diffraction data and refined structures. A.K., A.N., and M.L.C. performed the HTS. Y.L., H.Q.N., and C.K. carried out the NMR experiment and analysis. A.K. and X.K.-S. performed the thermal shift assay and SPR, respectively. K.F. and A.P. analyzed the chemical scaffolds and fitted the inhibitors to the electron density. A.M., J.L., J.H., and P.D. conceived of and coordinated the studies and participated in writing the manuscript.

Notes
The authors declare no competing financial interest.

■ ACKNOWLEDGMENTS

This research was supported by the National Research Foundation of Singapore through the Singapore-MIT Alliance for Research and Technology (SMART) Infectious Diseases and Antimicrobial Resistance Interdisciplinary Research Groups; SMART Innovation Centre Grant ING137070-BIO to P.D. and J.L.; the Biomedical Sciences Institutes (BMSI), Agency for Science, Technology, and Research (A*STAR), Singapore; and AcRF Grants Tier1 RG154/14 and MOE2015-T2-2-075 to J.L.

■ ABBREVIATIONS

Hi, *H. influenzae*; HTS, high-throughput screen; K_i, inhibitory constant; NTD, N-terminal domain; IC_{50}, half-maximal inhibitory concentration; MIC, minimum inhibitory concentration; *Pa*, *P. aeruginosa*; PDB, Protein Data Bank; RBCs, red blood cells; RLU, relative luminescence units; SAH, *S*-adenosyl-L-homocysteine; SAM, *S*-adenosyl-L-methionine; SPR, surface plasmon resonance; TrmD, tRNA-(N^1G37) methyltransferase; tRNA, transfer RNA; T_m, melting point

■ REFERENCES

(1) Bush, K., Courvalin, P., Dantas, G., Davies, J., Eisenstein, B., Huovinen, P., Jacoby, G. A., Kishony, R., Kreiswirth, B. N., Kutter, E., Lerner, S. A., Levy, S., Lewis, K., Lomovskaya, O., Miller, J. H., Mobashery, S., Piddock, L. J., Projan, S., Thomas, C. M., Tomasz, A., Tulkens, P. M., Walsh, T. R., Watson, J. D., Witkowski, J., Witte, W., Wright, G., Yeh, P., and Zgurskaya, H. I. (2011) Tackling antibiotic resistance. *Nat. Rev. Microbiol. 9* (12), 894−6.

(2) O'Neill, J. Antimicrobial Resistance: Tackling a crisis for the health and wealth of nations. 2014.

(3) Vogel, G. (2017) Meet WHO's dirty dozen: The 12 bacteria for which new drugs are most urgently needed. *Science*, DOI: 10.1126/science.aal0829.

(4) Centers for Disease Control and Prevention. Antibiotic Resistance Threats in the United States, 2013. 2013.

(5) Schaefer, M., Kapoor, U., and Jantsch, M. F. (2017) Understanding RNA modifications: the promises and technological bottlenecks of the 'epitranscriptome '. *Open Biol. 7* (5), 170077.

(6) Chionh, Y. H., McBee, M., Babu, I. R., Hia, F., Lin, W., Zhao, W., Cao, J., Dziergowska, A., Malkiewicz, A., Begley, T. J., Alonso, S., and Dedon, P. C. (2016) tRNA-mediated codon-biased translation in mycobacterial hypoxic persistence. *Nat. Commun. 7*, 13302.

(7) Gu, C., Begley, T. J., and Dedon, P. C. (2014) tRNA modifications regulate translation during cellular stress. *FEBS Lett. 588* (23), 4287−96.

(8) Masuda, I., Sakaguchi, R., Liu, C., Gamper, H., and Hou, Y.-M. (2013) The temperature sensitivity of a mutation in the essential tRNA modification enzyme tRNA methyltransferase D (TrmD). *J. Biol. Chem. 288* (40), 28987−28996.

(9) O'Dwyer, K., Watts, J. M., Biswas, S., Ambrad, J., Barber, M., Brulé, H., Petit, C., Holmes, D. J., Zalacain, M., and Holmes, W. M. (2004) Characterization of Streptococcus pneumoniae TrmD, a tRNA methyltransferase essential for growth. *J. Bacteriol. 186* (8), 2346−2354.

(10) Kobayashi, K., Ehrlich, S. D., Albertini, A., Amati, G., Andersen, K. K., Arnaud, M., Asai, K., Ashikaga, S., Aymerich, S., Bessieres, P., Boland, F., Brignell, S. C., Bron, S., Bunai, K., Chapuis, J., Christiansen, L. C., Danchin, A., Débarbouillé, M., Dervyn, E., Deuerling, E., Devine, K., Devine, S. K., Dreesen, O., Errington, J., Fillinger, S., Foster, S. J., Fujita, Y., Galizzi, A., Gardan, R., Eschevins, C., Fukushima, T., Haga, K., Harwood, C. R., Hecker, M., Hosoya, D., Hullo, M. F., Kakeshita, H., Karamata, D., Kasahara, Y., Kawamura, F., Koga, K., Koski, P., Kuwana, R., Imamura, D., Ishimaru, M., Ishikawa, S., Ishio, I., Le Coq, D., Masson, A., Mauël, C., Meima, R., Mellado, R. P., Moir, A., Moriya, S., Nagakawa, E., Nanamiya, H., Nakai, S., Nygaard, P., Ogura, M., Ohanan, T., O'Reilly, M., O'Rourke, M., Pragai, Z., Pooley, H. M., Rapoport, G., Rawlins, J. P., Rivas, L. A., Rivolta, C., Sadaie, A., Sadaie, Y., Sarvas, M., Sato, T., Saxild, H. H., Scanlan, E., Schumann, W., Seegers, J. F. M. L., Sekiguchi, J., Sekowska, A., Séror, S. J., Simon, M., Stragier, P., Studer, R., Takamatsu, H., Tanaka, T., Takeuchi, M., Thomaides, H. B., Vagner, V., van Dijl, J. M., Watabe, K., Wipat, A., Yamamoto, H., Yamamoto, M., Yamamoto, Y., Yamane, K., Yata, K., Yoshida, K., Yoshikawa, H., Zuber, U., and Ogasawara, N. (2003) Essential Bacillus subtilis genes. *Proc. Natl. Acad. Sci. U. S. A. 100* (8), 4678−4683.

(11) Björk, G. R., Jacobsson, K., Nilsson, K., Johansson, M. J., Byström, A. S., and Persson, O. P. (2001) A primordial tRNA modification required for the evolution of life? *EMBO J. 20* (1−2), 231−239.

(12) Hill, P. J., Abibi, A., Albert, R., Andrews, B., Gagnon, M. M., Gao, N., Grebe, T., Hajec, L. I., Huang, J., Livchak, S., Lahiri, S. D., McKinney, D. C., Thresher, J., Wang, H., Olivier, N., and Buurman, E. T. (2013) Selective inhibitors of bacterial t-RNA-(N(1)G37) methyltransferase (TrmD) that demonstrate novel ordering of the lid domain. *J. Med. Chem. 56* (18), 7278−88.

(13) Goto-Ito, S., Ito, T., Kuratani, M., Bessho, Y., and Yokoyama, S. (2009) Tertiary structure checkpoint at anticodon loop modification in tRNA functional maturation. *Nat. Struct. Mol. Biol. 16* (10), 1109−1115.

(14) Eram, M. S., Bustos, S. P., Lima-Fernandes, E., Siarheyeva, A., Senisterra, G., Hajian, T., Chau, I., Duan, S., Wu, H., Dombrovski, L., Schapira, M., Arrowsmith, C. H., and Vedadi, M. (2014) Trimethylation of Histone H3 Lysine 36 by Human Methyltransferase PRDM9 Protein. *J. Biol. Chem. 289* (17), 12177−12188.

(15) Duan, J., Dixon, S. L., Lowrie, J. F., and Sherman, W. (2010) Analysis and comparison of 2D fingerprints: insights into database screening performance using eight fingerprint methods. *J. Mol. Graphics Modell. 29* (2), 157−70.

(16) Sastry, M., Lowrie, J. F., Dixon, S. L., and Sherman, W. (2010) Large-scale systematic analysis of 2D fingerprint methods and parameters to improve virtual screening enrichments. *J. Chem. Inf. Model. 50* (5), 771−84.

(17) Li, Y., Zhong, W., Koay, A. Z., Ng, H. Q., Ngo, A., Koh-Stenta, X., Nah, Q., Lim, S. H., Larsson, A., Keller, T. H., Lescar, J., Hill, J.,

DOI: 10.1021/acsinfecdis.8b00275
ACS Infect. Dis. 2019, 5, 326−335

Dedon, P. C., and Kang, C. B. (2018) Backbone resonance assignment for the N-terminal region of bacterial tRNA-(N1G37) methyltransferase. *Biomol. NMR Assignments 10*, 135−138.
(18) Jaroensuk, J., Wong, Y. H., Zhong, W., Liew, C. W., Maenpuen, S., Atichartpongkul, S., Chionh, Y. H., Nah, Q., Thongdee, N., McBee, M. E., Prestwich, E. G., DeMott, M. S., Chaiyen, P., Mongkolsuk, S., Dedon, P. C., Lescar, J., and Fuangthong, M. (2018) Crystal structure and catalytic mechanism of the essential m1G37 tRNA methyltransferase TrmD from *Pseudomonas aeruginosa*. *RNA*, n/a.
(19) Ito, T., Masuda, I., Yoshida, K.-i., Goto-Ito, S., Sekine, S.-i., Suh, S. W., Hou, Y.-M., and Yokoyama, S. (2015) Structural basis for methyl-donor-dependent and sequence-specific binding to tRNA substrates by knotted methyltransferase TrmD. *Proc. Natl. Acad. Sci. U. S. A. 112* (31), E4197−205.
(20) Richter, M. F., Drown, B. S., Riley, A. P., Garcia, A., Shirai, T., Svec, R. L., and Hergenrother, P. J. (2017) Predictive compound accumulation rules yield a broad-spectrum antibiotic. *Nature 545* (7654), 299−304.
(21) Zhang, J.-H., Chung, T. D., and Oldenburg, K. R. (1999) A Simple Statistical Parameter for Use in Evaluation and Validation of High Throughput Screening Assays. *J. Biomol. Screening 4* (2), 67−73.
(22) Cer, R. Z., Mudunuri, U., Stephens, R., and Lebeda, F. J. (2009) IC50-to-Ki: a web-based tool for converting IC50 to Ki values for inhibitors of enzyme activity and ligand binding. *Nucleic Acids Res. 37* (Web Server), W441−W445.
(23) Li, Y., Wong, Y. L., Ng, F. M., Liu, B., Wong, Y. X., Poh, Z. Y., Liu, S., Then, S. W., Lee, M. Y., Ng, H. Q., Huang, Q., Hung, A. W., Cherian, J., Hill, J., Keller, T. H., and Kang, C. (2016) Escherichia coli Topoisomerase IV E Subunit and an Inhibitor Binding Mode Revealed by NMR Spectroscopy. *J. Biol. Chem. 291* (34), 17743−17753.
(24) Battye, T. G. G., Kontogiannis, L., Johnson, O., Powell, H. R., and Leslie, A. G. W. (2011) iMOSFLM: a new graphical interface for diffraction-image processing with MOSFLM. *Acta Crystallogr., Sect. D: Biol. Crystallogr. 67* (Part 4), 271−281.
(25) Evans, P. (2006) Scaling and assessment of data quality. *Acta Crystallogr., Sect. D: Biol. Crystallogr. 62* (1), 72−82.
(26) Evans, P. R., and Murshudov, G. N. (2013) How good are my data and what is the resolution? *Acta Crystallogr., Sect. D: Biol. Crystallogr. 69* (7), 1204−1214.
(27) McCoy, A. J., Grosse-Kunstleve, R. W., Adams, P. D., Winn, M. D., Storoni, L. C., and Read, R. J. (2007) Phaser crystallographic software. *J. Appl. Crystallogr. 40* (Part 4), 658−674.
(28) Emsley, P., and Cowtan, K. (2004) Coot: model-building tools for molecular graphics. *Acta Crystallogr., Sect. D: Biol. Crystallogr. 60* (12), 2126−2132.
(29) Murshudov, G. N., Skubák, P., Lebedev, A. A., Pannu, N. S., Steiner, R. A., Nicholls, R. A., Winn, M. D., Long, F., and Vagin, A. A. (2011) REFMAC5 for the refinement of macromolecular crystal structures. *Acta Crystallogr., Sect. D: Biol. Crystallogr. 67* (4), 355−367.
(30) Schüttelkopf, A. W., and van Aalten, D. M. F. (2004) PRODRG: a tool for high-throughput crystallography of protein-ligand complexes. *Acta Crystallogr., Sect. D: Biol. Crystallogr. 60* (Part 8), 1355−1363.
(31) Davis, I. W., Leaver-Fay, A., Chen, V. B., Block, J. N., Kapral, G. J., Wang, X., Murray, L. W., Arendall, W. B., Snoeyink, J., Richardson, J. S., and Richardson, D. C. (2007) MolProbity: all-atom contacts and structure validation for proteins and nucleic acids. *Nucleic Acids Res. 35* (Web Server), W375−W383.
(32) *The PyMOL Molecular Graphics System*, version 1.8; Schrödinger, LLC, 2015.
(33) Stierand, K., Maass, P. C., and Rarey, M. (2006) Molecular complexes at a glance: automated generation of two-dimensional complex diagrams. *Bioinformatics 22* (14), 1710−1716.
(34) Fricker, P. C., Gastreich, M., and Rarey, M. (2004) Automated Drawing of Structural Molecular Formulas under Constraints. *J. Chem. Info Comp Sci. 44* (3), 1065−1078.

DOI: 10.1021/acsinfecdis.8b00275
ACS Infect. Dis. 2019, 5, 326−335